J. Fluid Mech. (1982), *vol.* 123, *pp.* 69–90
Printed in Great Britain

On the spreading of a turbulent spot in the absence of a pressure gradient

By I. WYGNANSKI, M. ZILBERMAN
School of Engineering, Tel-Aviv University

AND JOSEPH H. HARITONIDIS†
Department of Aerospace Engineering, University of Southern California

(Received 25 August 1980 and in revised form 1 October 1981)

Velocity measurements in the plane of symmetry of a turbulent spot are reported. The number of data points taken at various streamwise locations was adequate to map the ensemble-averaged flow field in a spot at a given instance. These results are compared with velocities taken in laboratory coordinates (i.e. at a given station with variable time), whereupon it is shown that the flow field in the spot depends either on the distance from its origin or on the time elapsed from its initiation. The two variables are related so that the flow may be transformed into either a time- or a space-independent problem. The dependence of the spot on the Reynolds number and on the surrounding laminar boundary layer is established. The effects of these parameters on the shape of the ensemble-averaged spot, its size, characteristic celerities, and relative rate of entrainment, are discussed.

The present results indicate that a similarity approach based on ensemble-averaged data is severely limited. It might be used to predict the overall scales and flow field but much more sophisticated data-processing techniques are required to describe the structure of the spot.

1. Introduction

Transitional spots have been investigated for several years because of their role in the generation of a turbulent boundary layer. Pictures of spots, using various techniques of flow visualization (Gad-el-Hak, Blackwelder & Riley 1980, 1981), reveal that the spot contains a number of eddies, and thus may be more than just a prototype of a single, large coherent structure (see insert in figure 18). Furthermore, an isolated spot in a laminar boundary layer grows indefinitely in both streamwise and spanwise directions, and its dimensions are not comparable with any reasonable boundary-layer scales. The substructures within the spot cannot occur entirely at random in view of the universality of the spot's shape and spreading angle.

However, if any portion of the spot is to serve as a prototype of the large coherent eddy in a turbulent boundary layer, its aggregate kinematics and dynamics should be modelled and made amenable to analysis. One possible parameter associated with the kinematics of the spot is the rate at which the spot entrains non-turbulent fluid. The spot, being regarded as a time-dependent, three-dimensional structure, cannot be easily described mathematically without making some simplifying assumptions. One very powerful and successful method in boundary-layer theory is the assumption

† Present address: Department of Aeronautics and Astronautics, Massachusetts Institute of Technology.

of similarity, which was applied to the spot by Cantwell, Coles & Dimotakis (1978, hereinafter referred to as CCD). By looking at some characteristic features of the ensemble-averaged velocity traces in and around a turbulent spot, CCD concluded that the spot grows conically. The assumption of conical similarity enabled CCD to collapse some characteristic loci in the velocity traces, measured at two streamwise locations, onto a single curve, thus confirming the concept and defining similarity coordinates η and ξ (where $\eta = y/U_\infty t$; $\xi = x/U_\infty t$; t being time; x and y are distances in directions respectively parallel and normal to the surface). All quantities are measured from a virtual origin of the flow. In these coordinates, Galilean-invariant particle paths were obtained that enabled the authors to calculate the local rate of entrainment on the plane of symmetry of an ensemble-averaged spot. The particle trajectories led CCD to conclude that the ensemble-averaged spot contains two vortices that serve as points of accumulation of the fluid entrained by the spot.

Wygnanski, Sokolov & Friedman (1976, hereinafter referred to as WSF), realized that the shape of an ensemble-averaged spot is self-similar, provided that the length of the spot at the wall and the maximum height of the spot are used as normalizing lengthscales. They proceeded to show that the length of the spot should scale linearly with the distance from the location of the disturbance to the measuring station. They also observed that the duration of the spot at a fixed location in its plane of symmetry scales linearly with the same distance. This scaling provides the transformation between time and space and enables one to interpret measurements made in laboratory coordinates to space coordinates associated with the spot. Schubauer & Klebanoff (1956, hereinafter referred to as SK) suggested that the height of the spot scales approximately as the height of the hypothetical turbulent boundary layer originating at the spark with an initial thickness equal to the thickness of the laminar boundary layer at that location. The data of WSF agree with the suggestion made by SK implying that the *laminar boundary layer plays a role* in determining the initial shape of the spot and, to some extent, its final height. In fact, it is inconceivable that a transitional spot will be totally independent of the laminar boundary layer in which it is embedded and on whose vorticity it must feed.

A detailed comparison between the conical-similarity approach of CCD and the experimental investigation of WSF reveals a number of basic differences, which should be reconciled if the spot or some part of it is to serve for modelling the large coherent structure in turbulent-boundary-layer calculations. Some of the major differences are as follows.

(i) It may be inferred from the measurements made by CCD that a single length measured from a uniquely defined origin suffices to scale the spot reasonably well in every direction. SK and WSF suggested that the streamwise variation of the height of the spot is similar to that of a turbulent boundary layer, while the length and the span of the spot increase linearly with distance from the perturbation. The virtual origin in each direction may also be different.

(ii) The conical similarity neglects, to the first approximation, the effects of the background laminar boundary layer. SK, as well as WSF, suggest some relationship between the shape of the spot and the laminar boundary layer. To date, the importance of these effects appeared to be secondary, because neither CCD nor WSF considered the consequences of variable Reynolds number on the growth of the spot.

(iii) The conical-similarity approach presumes that every point on the interface of the spot moves with its own characteristic celerity because the length of each interface increases with downstream distance. According to WSF, the celerities of the leading and trailing interfaces on the plane of symmetry of the spot did not vary with distance

from the surface. Thus the flow, relative to an observer moving with the interface, should have been steady.

The purpose of this investigation was to provide additional data on the rate of growth of the transitional spot, which may help to resolve the discrepancies between the interpretation of the measurements reported by CCD and WSF, in particular with regard to the relationship between *temporal* and *spatial* rates of growth of the spot. Furthermore, the dependence of some characteristic features of the transitional spot on Reynolds number has to be investigated.

2. Results and discussion

The apparatus used in this experiment, the measuring equipment and the methods of data acquisition and reduction are described in an earlier paper (Wygnanski, Haritonidis & Kaplan 1979), and thus the description will not be repeated here.

2.1. *On the spreading property of the spot*

Figure 1 shows a typical record of velocity perturbation measured at a station $x_m - x_s = 1100$ mm downstream of the spark and 1400 mm downstream of the leading edge of the plate. The free-stream velocity U_∞ was 10 m/s. The abscissa in this figure is time, starting 70 ms after the occurrence of the spark and ending 204·8 ms later. Each trace in the figure represents velocity measured at a different elevation above the plate from 1 mm above the surface to 25·4 mm from the wall. The velocity history across the entire cross-section of the spot is thus recorded for every realization. The local velocity prevailing in the laminar flow is subtracted from each record in order to facilitate the presentation. When 200 events are ensemble-averaged, the turbulent (high-frequency) fluctuations occurring at random during each realization disappear, leaving a fairly smooth record of the average perturbation velocity during a passage of a spot (figure 2).

Records similar to figure 2 were presented by WSF and CCD. The ensemble-averaged velocity record marking the spot can be characterized by a defect in velocity at the outer edge of the boundary layer and an excess of velocity near the surface. CCD suggested that each record was well represented by several straight-line segments intersecting at points labelled A–G (see figure 12 of CCD). Some of the most clearly identifiable corresponding points are marked in figure 2 for the purposes of orientation. From the record shown, one may choose four characteristic features on the boundary of the spot and determine the time of their occurrence. These points mark the following locations:

(i) the leading edge of the spot near the surface;

(ii) the most forward-reaching position of the leading interface (the overhang); loci 1 and 2 correspond to locus A shown in figure 12 of CCD;

(iii) the location of the maximum height of the spot (corresponds to locus C of CCD);

(iv) the trailing edge of the spot near the surface (locus F of CCD)

By repeating the measurement at numerous streamwise locations on the plane of symmetry of the spot, the points labelled 1–4 occur at different times, which are determined by the location of the probe. These loci are plotted in (x, t)-coordinates (figure 3), in a manner suggested by CCD. Data from 9 measuring stations are shown in figure 3 for streamwise locations varying from 800–1500 mm downstream of the spark. The loci marked may be connected by straight lines, whose slopes represent the streamwise component of the celerity of the particular features chosen. The celerity of loci 1 and 2 is $0{\cdot}89U_\infty$ and of locus 3 is not appreciably different ($0{\cdot}82U_\infty$

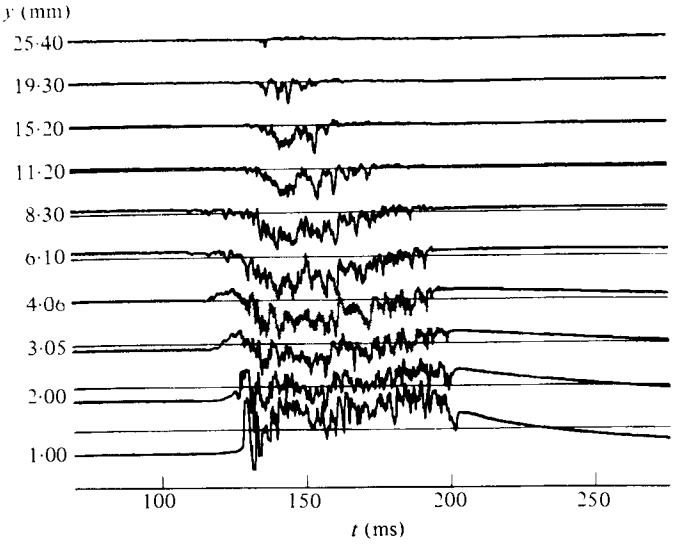

FIGURE 1. A single record of velocity perturbation across the spot at $x_m - x_0 = 1030$ mm, $z = 0$, $U_\infty = 10$ m/s, $x_s = 300$ mm.

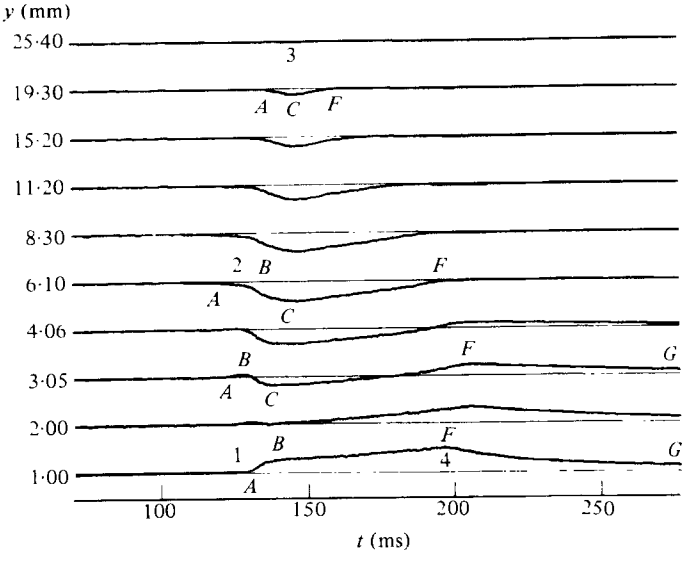

FIGURE 2. An ensemble-averaged velocity perturbation across the spot at $x_m - x_0 = 1030$, $z = 0$, $U_\infty = 10$ m/s, $x_s = 300$ mm.

for the data shown in figure 3, and $0{\cdot}89U_\infty$ for the data taken at 19 m/s and shown in figure 15). The celerity of locus 4 is $0{\cdot}57U_\infty$. Loci 1, 2 and 3 are situated on the leading interface of the spot. Thus one may assume that the leading interface on the plane of symmetry moves downstream with approximately constant velocity independent of y (y being the distance from the surface). Furthermore, the inclination and shape of the leading interface does not vary with increasing distance from the spark.

The contours $U - U_{\text{lam}}/U_\infty = -0{\cdot}02$, which may represent the boundaries of the

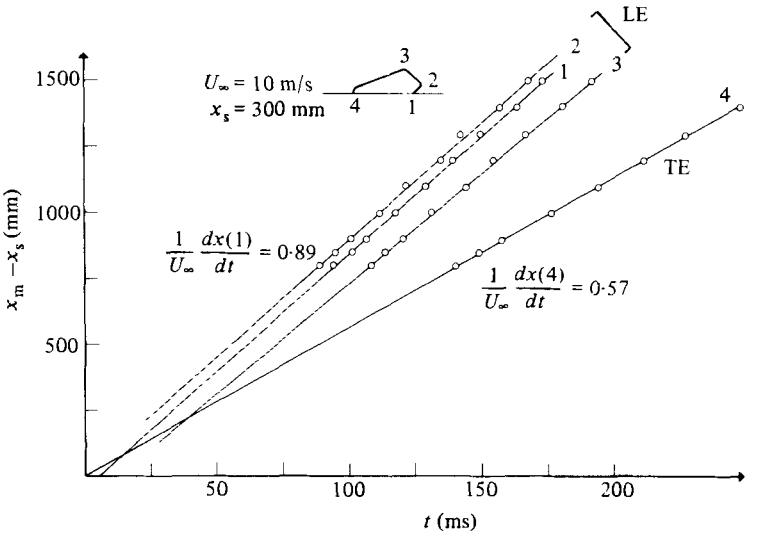

FIGURE 3. The determination of the celerity of some observable features of the spot.

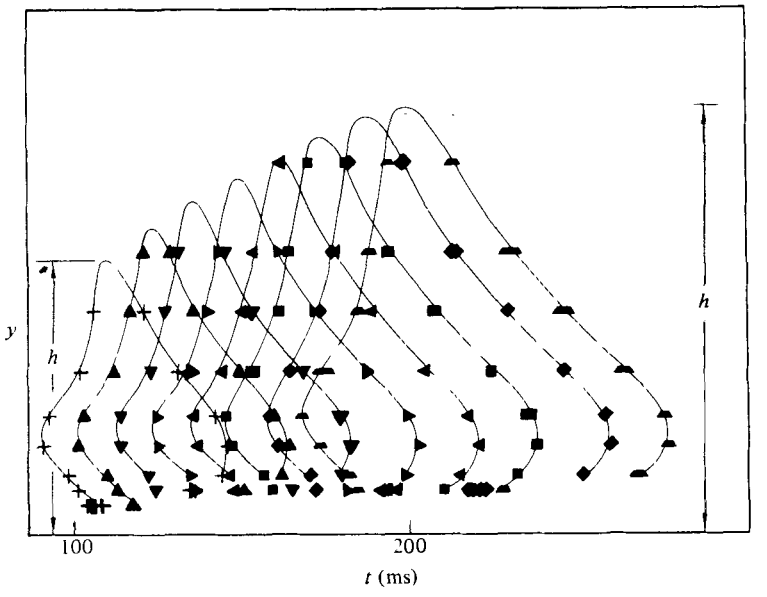

FIGURE 4. Perturbation contours $(U-U_{\text{lam}})/U_\infty = -2\%$ plotted in (y,t)-coordinates.

spot outside the laminar boundary layer, are shown in figure 4. The streamwise separation between adjacent contours is 100 mm. This determination of the spot's boundary was first used by Coles & Barker (1975), and is repeated here for the sake of convenience; a detailed comparison between this criterion and the actual determination of the turbulent–non-turbulent interface is discussed by WSF. Even if the contour $U-U_{\text{lam}}/U_\infty = -0{\cdot}02$ does not coincide with the interface of the spot it is an unbiased characteristic feature of the spot near its outer boundary. One may

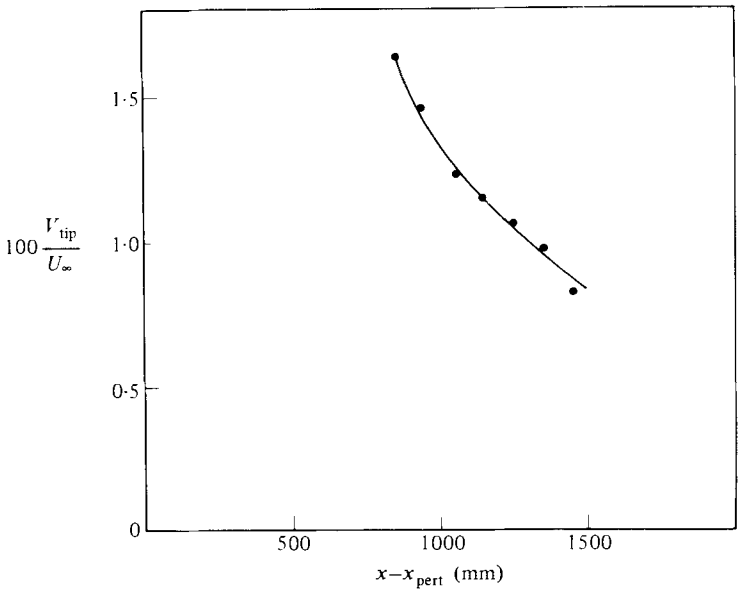

FIGURE 5. The variation with x of the normal velocity of the apex of the spot; $U_\infty = 10$ m/s, $x_s = 300$ mm.

deduce from figure 4 that the boundaries of adjacent spots are approximately parallel, which could lead to the notion that the celerity of the trailing interfaces in the x-direction is *locally* independent of y. In order to compare the celerity of the trailing interface over long downstream distances, one has to account for the growth of the spot in the y-direction as well. It should be remembered, however, that the coordinates used in figure 4 accentuate the height of the spot, which is physically a very flat structure.

The variation of the maximum height of the spot with x can be roughly estimated from figure 4; and from it one may calculate the outward propagation velocity of the tip (figure 5). The forward 'overhang' of the spot (locus 2) does not propagate outwards, in the range of the measurements shown; and it is roughly located at $y = 7$ mm from the surface of the plate. It may be assumed that the normal component of the interface celerity increases linearly with the normal distance from the overhang. Thus

$$\frac{V_{\text{interface}}}{V_{\text{tip}}} = \frac{y - y_{\text{overhang}}}{h - y_{\text{overhang}}},$$

where h is the maximum height of the spot. Taking advantage of the general similarity of the spot boundaries, one may calculate the streamwise component of the celerity of the trailing interface at similar locations on the boundary, thus accounting for the growth of the spot in the y-direction. Using the data shown in figure 4 leads to the conclusion that U_{TE} accelerates with increasing y (see table 1). In fact, only the lower portion of the trailing interface is convected at a constant celerity. These results differ from the conclusion of WSF, who suggested that the celerity of each interface is constant in the plane of symmetry of the spot. The difference may stem from the fact that the measurements were made locally, mostly at the lower part ($y/h \leqslant 0{\cdot}5$) of the spot (see figure 10 of WSF).

The present results, however, do not confirm the assumption of conical similarity because the lines passing through loci 1, 2, 3 and 4 (in figures 3 and 15) do not converge

even approximately to a common origin. The difference between the celerities of the leading and trailing interface is associated with the spatial growth of the spot. In fact, the length of the spot almost doubles between $x_m = 800$ mm and $x_m = 1500$ mm corresponding to the two extreme locations shown in figure 3. The lines connecting loci 1 and 4 intersect at $t_0 = 12$ ms and $x_0 - x_s = 70$ mm, which may represent a virtual origin of the spot at the wall. However, since loci 2 and 3 do not intersect 4 at the same point as 1, there is thus no uniquely defined virtual origin for the spot. One may choose the intersection of 2 and 4 for the virtual origin because these loci represent the extreme streamwise extent of the spot, although the elevation of locus 2 coincides roughly with the edge of the laminar boundary layer. It is known (Kovasznay, Komoda & Vasudeva 1962) that the breakdown to turbulence originates at the outer part of the laminar boundary layer, favouring perhaps the choice of 2. One may also choose the origin of the spot at the intersection of locus 3 with either one of the principal axes (t or x). Locus 3, if it were to exist in a single realization, would represent a singular point at the intersection of the leading and trailing interfaces. In the following discussion x_0 and t_0 were always determined from the intersection of loci 1 and 4. Although this choice is arbitrary, it has no appreciable influence on collapsing a limited set of data measured far downstream.

In the absence of the conical property, the similarity coordinates $\xi = x/U_\infty t$ and $\eta = y/U_\infty t$ (where x, y and t are independent variables) are not appropriate, because they imply that the spot can be scaled by a single lengthscale $U_\infty t$. Nevertheless, it is still possible that every characteristic feature of the spot is convected downstream with a constant celerity so that the ratio $(x_m - x_0)/U_\infty(t_m - t_0)$, representing this feature and its own virtual origin $(x_0; t_0)$ be constant. Assuming that the results far downstream are insensitive to the choice of x_0 and t_0, one may fix the virtual origin at the intersection of 1 and 4 and check whether a single scaling factor will relate measurements made in laboratory coordinates (i.e. at fixed x but varying time) to spatial measurements made at a given time. The latter would be equivalent to a photographic record showing the instantaneous flow in and around the spot. Having measured the ensemble-averaged velocity distribution at 9 streamwise locations, one can compare the temporal velocity record taken at any location in the flow during the passage of the spot, with the velocity measured at a given time at all 9 locations. The first column of $\times$-symbols on the left-hand side of figure 6(a) represents the velocity at the furthest streamwise location measured (i.e. at $x_m - x_0 = 1430$ mm), at the particular time chosen. At that time, the spot was about to arrive at this location. The last column of symbols in this figure represents a velocity at $x_m - x_0 = 730$ mm; at the chosen time the trailing interface of the spot had passed this measuring station and is roughly located at $x_m - x_0 = 880$ mm near the surface of the plate.

For the purpose of comparison with a temporal record measured in laboratory coordinates, each row of $\times$-symbols in figure 6(a) represents a perturbation velocity occurring at a given relative elevation in a spot whose apex is located at $x_m - x_0 = 1430$ mm. Namely, the ratio y/h is constant for each row of symbols in spite of the fact that the maximum height h of the spot increases in the streamwise direction and the measurements were made with a rake of wires located at fixed distances from the surface. This was achieved by interpolating the velocity measured by adjacent wires in the y-direction.

The solid lines shown in figure 6(a) represent the temporal velocity records at $x_m - x_0 = 1430$ mm. Each temporal record shown, being measured at a constant elevation above the plate, corresponds automatically to a constant y/h at $x_m - x_0 = 1430$ mm. The comparison was made after the temporal record was multiplied by $CU_\infty/(x_m - x_0)$, where $x_m - x_0$ is the distance of the measuring station from the

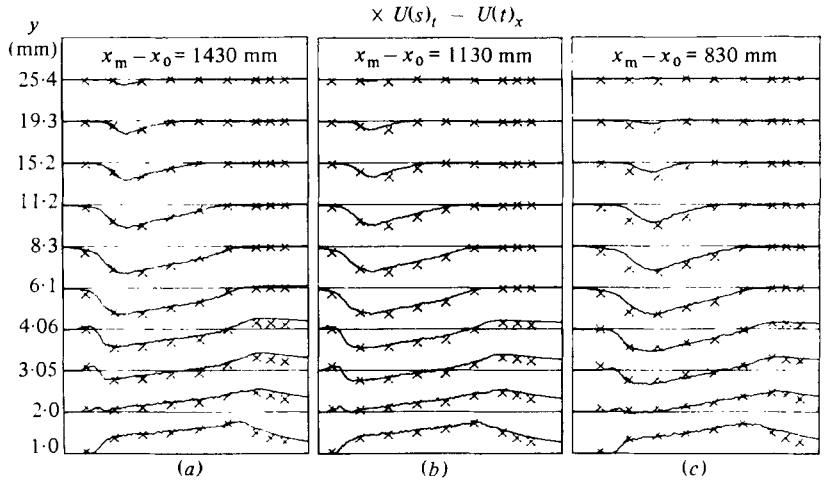

FIGURE 6. A comparison between a temporal velocity-perturbation record at a fixed measuring station and a spatial velocity-perturbation record at a fixed time; $U_\infty = 10$ m/s, $x_s = 300$ mm. Distance between horizontal reference lines corresponds to $(U-U_{\text{lam}})/U_\infty = 0{\cdot}5$.

chosen origin of the flow, and C is a constant. The agreement between the two types of measurements is fairly good, although the temporal record presented in figure 6(*a*) corresponds to a time period starting with the arrival of the spot at $x_m - x_0 = 1430$ mm, while the spatial data end at this location. Thus, the spatial data obtained at various upstream stations can be used to predict the temporal flow field during the passage of the spot. On the other hand, the temporal velocity record shown in figure 6(*c*), which was measured at $x_m - x_0 = 830$ mm, agrees fairly well with the spatial velocity record, which extends to the last measuring station at $x_m - x_0 = 1430$ mm. This agreement can be used to predict the 'instantaneous' (ensemble-averaged) flow field associated with a spot that has already passed the measuring station.

The temporal record presented in figure 6(*b*) was measured at $x_m - x_0 = 1130$ mm. At this streamwise distance the elapsed time of 172 ms after the initiation of the spot occurs roughly at the centre of the temporal record near the surface; thus the comparison between the velocity perturbations $U(t)$ obtained in laboratory coordinates and those $U(x)$ obtained instantaneously in space is most appropriate. The agreement between the two sets of data in this case is good. All three temporal records in figure 6 were multiplied by a constant velocity and scaled by a distance from an arbitrarily determined single hypothetical origin in spite of the fact that the latter is not unique (figure 3). Thus, if the temporal record predicting the instantaneous velocity perturbation associated with a spot could be scaled by a different $x_m - x_0$, this would result in better agreement between the two velocity records shown in figures 6(*a*, *c*). The non-existence of a uniquely defined x_0 indicates that similarity arguments are approximate at best.

It is important to note from figure 6 that the dimensionless length of the spot at a given time is proportional to the dimensionless duration of the spot at a given measuring station, i.e.

$$\frac{l}{U_\infty(t_m - t_0)} \propto \frac{\Delta t\, U_\infty}{x_m - x_0},$$

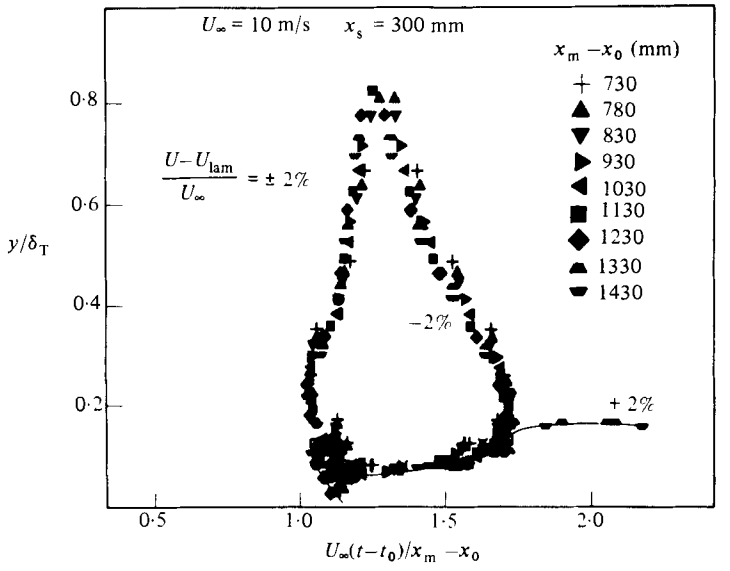

FIGURE 7. Perturbation contours $(U-U_{\text{lam}})/U_\infty = +2\%$ plotted in the suggested similarity coordinates.

where l is the length of the spot, Δt is the duration of the spot, t_m is the time of measurement and x_m is the location of measurement. The value of $l(x_m-x_0)/U_\infty^2\,\Delta t(t_m-t_0)$ for the data presented in figure 3 is 0·48. Furthermore, any feature ascribed to the ensemble-averaged velocity field and measured in the laboratory coordinates (at fixed $x = x_m$) and variable time will be observed at a given time at some (variable x) location in the flow. *Consequently, the variables x and t are related in this flow.* Since it is more convenient to use laboratory coordinates at which x is fixed, the similarity timescale of the problem becomes $(x_m-x_0)/U_\infty$, by which temporal velocity records obtained at any measuring station could be scaled. *This scale applies to every measuring station as long as the Reynolds number at the location of the spark is held constant.*

The maximum height h of the spot increases in the downstream direction, as may be seen from the three temporal records shown in figure 6. At $x_m-x_0 = 1430$ mm the spot extends beyond $y = 25{\cdot}4$ mm (figure 6*a*), while at $x_m-x_0 = 830$ mm its tip, as may be detected from the perturbation in velocity, does not extend much beyond 19 mm (figure 6*c*). Schubauer & Klebanoff (1956) suggested that the rate of growth of the spot in the y-direction is proportional to the growth rate of a turbulent boundary layer developing downstream of the spark, with an initial thickness equal to the thickness of the laminar boundary layer at the spark. This suggestion agreed with the results of WSF, and hence was tried in the present context. It seems reasonable to assume for this purpose that the turbulent-boundary-layer thickness may be represented by a power law, thus $\delta_T = 0{\cdot}37(x_m-x_1)^{\frac{4}{5}}(\nu/U_\infty)^{\frac{1}{5}}$, where δ_T is the thickness of a turbulent boundary layer and x_1 is determined by equating $\delta_T = \delta_{LS} = 5x_s^{\frac{1}{2}}(\nu/U_\infty)^{\frac{1}{2}}$, where x_s is the distance of the spark from the leading edge of the plate and δ_{LS} represents the laminar-boundary-layer thickness at the spark. For $U_\infty = 10$ m/s and $x_s = 300$ mm from the leading edge x_1 is 80 mm upstream of the spark.

The perturbation contours $U-U_{\text{lam}}/U_\infty = \mp 0{\cdot}02$ plotted in figure 7 were

obtained after distances measured from the wall were scaled by δ_T and the time by the characteristic timescale $(x_m - x_0)/U_\infty$ at the measuring station. The various symbols shown in the figure represent different measuring stations starting 800 mm downstream of the spark and ending 700 mm further downstream. The collapse onto a single curve is fairly good, indicating that the variables chosen to scale the spot are reasonable. Since both positive and negative perturbation contours are shown, the concentration of symbols near the surface is due to the fact that, at 2–4 mm from the plate, the ensemble-averaged velocity perturbation first becomes positive, then negative, and then positive again. The positive perturbation contours are marked by open symbols while the negative ones are marked by filled ones; the former are hardly distinguishable in view of the large number of symbols piling one on top of one another. Choosing different features to determine a pseudo-virtual origin of the spot improves the collapse of the data associated with the particular feature chosen, but the differences are not significant enough to warrant a preference of one choice upon another. They do indicate, however, that every characteristic feature of the spot may be traced to its own virtual origin. The deviations from similarity are attributed to the fact that the spot is embedded in a laminar boundary layer and the destabilization of this layer is governed by different scaling laws. Other perturbation contours given by $|U - U_{lam})/U_\infty| > 0{\cdot}02$ also collapse the data measured at different x-stations onto a single curve because the entire velocity-perturbation field inside the spot scales with the chosen parameters.

The same data, when scaled only by $U_\infty(t-t_0)$ (i.e. $\xi = (x_m - x_0)/(t-t_0)\,U_\infty$; $\eta = y/(t-t_0)\,U_\infty$), do not collapse as well onto a single curve (figure 8) regardless of the choice of virtual origin. This is particularly true at the outer part of the laminar boundary layer, where an increase in downstream distance causes an apparent shrinkage of the spot. Figure 3 shows that the height of the 'overhang' (i.e. the most-forward portion of the leading interface) varies by 50 % when one compares data taken at $x_m - x_0 = 830$ mm with data taken at $x_m - x_0 = 1430$ mm. One may improve the collapse of the data by expressing the boundary-layer thickness used for scaling y in terms of $U_\infty(t-t_0)$. Recent data of Savas (1979, see also Wygnanski 1981*a*) suggests that the height of the spot does not scale linearly with downstream distance but rather with $(x-x_0)^{0{\cdot}8}$.

We may now examine the flow at a particular station by plotting the data in a coordinate system

$$X = \frac{U_\infty(t-t_0)}{x_m - x_0}, \quad Y = \frac{y}{\delta_T},$$

where

$$\delta_T = \delta(x_m - x_0),$$

knowing reasonably well that this representation is valid for the entire flow field at any given time. Contours of constant velocity perturbation $(U - U_{lam})/U_\infty = C$ imply that the spot is represented by a family of closed loops of velocity defect riding above contours representing an excess of velocity (figure 9). The velocity-defect region coincides with the turbulent region in the spot, while the excess region has its maximum near the rear of the spot and is trailing behind it. The maximum perturbation velocity associated with the spot is approximately $\mp 30\,\%$ of U_∞.

One would like to know the mechanism that is responsible for the growth of the spot in both spanwise and streamwise directions, but, in attempting to achieve this goal, one has first to determine the region that most actively entrains non-turbulent fluid. The most obvious first step is to consider the entrainment into an ensemble-

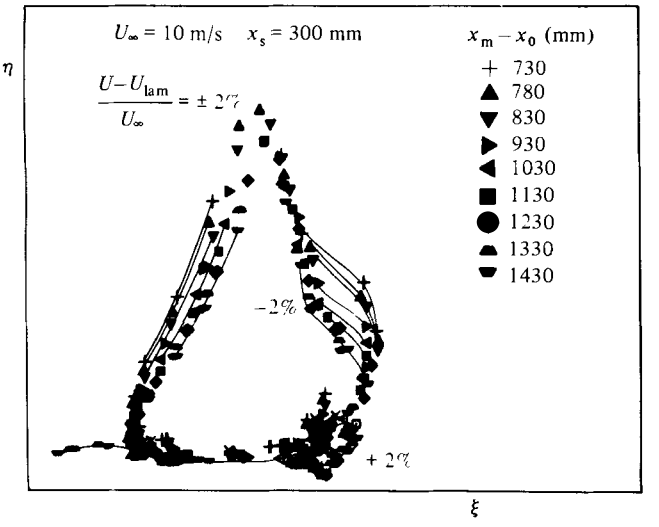

FIGURE 8. Perturbation contours $(U-U_{\text{lam}})/U_\infty = \pm 2\%$ plotted in the coordinates suggested by CCD.

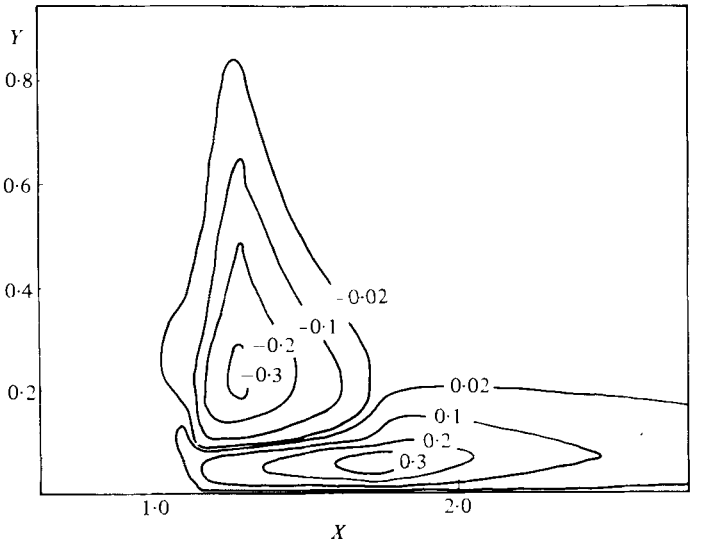

FIGURE 9. Details of velocity-perturbation contours measured at $x_m - x_0 = 930$ mm, $U_\infty = 10$ m/s.

averaged spot on its plane of symmetry. For this purpose, one should know the shape of the interface and the velocity field relative to it. The task is simple in principle, but requires tedious and difficult measurements. The first attempt was made by WSF, who measured the celerity of the leading and trailing interfaces locally and calculated the function $\int_0^y (U-U_{\text{interface}})\,dy$ relative to the respective interface. Inferring the entrainment from this procedure implies that the flow relative to the interface is steady and two-dimensional (i.e. $(\partial W/\partial z)_{z=0} = 0$). Furthermore, the growth of the

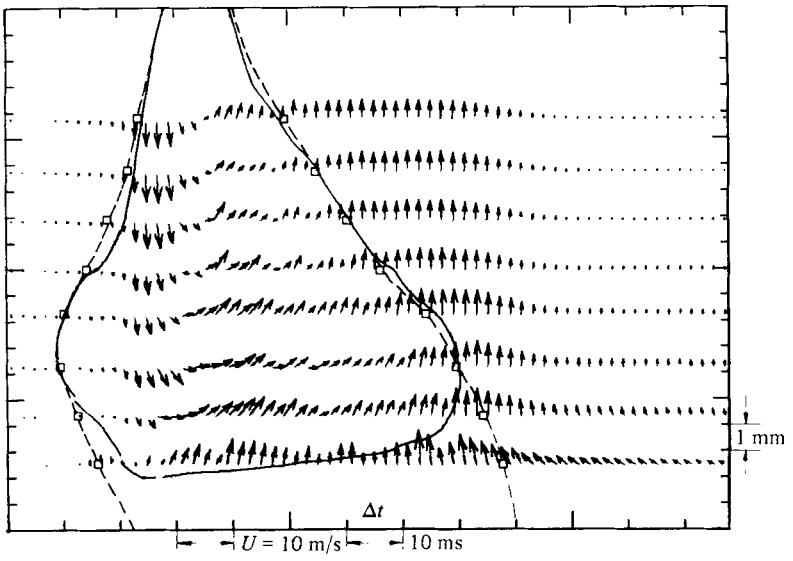

FIGURE 10. Measured velocity-perturbation vectors in a transition spot; $x_s = 300$ mm, $x_m - x_0 = 1030$ mm, $U_\infty = 10$ m/s. See text for scales.

spot in the y-direction has been neglected. CCD argued that in laboratory coordinates the stream function depends on x, y and t and thus has a total differential

$$d\psi = -V\,dx + U\,dy + \frac{\partial \psi}{\partial t}\,dt,$$

which includes a time-dependent term. Consequently the integration of $U - U_{\text{interface}}$ with respect to y is insufficient to calculate entrainment. They estimated the rate of entrainment by assuming conical similarity and calculating the particle trajectories relative to an interface.

In the present context an attempt is made to calculate the rate of entrainment directly from measurements, without resorting to the assumption of two-dimensionality, conical similarity or the invariance of leading-edge celerity with y. The average velocity field within the spot and its vicinity was measured with a rake of X-wires. The velocity perturbation vectors in the (y, t)-plane are shown in figure

Level	y (mm)	U_{LE}/U_∞	U_{TE}/U_∞	$(V_{int}/U_\infty) \times 10^3$
1	2·46	0·9	0·55	0
2	4·34	0·9	0·55	0
3	6·21	0·9	0·55	0
4	8·21	0·9	0·59	1·18
5	9·96	0·85	0·63	2·90
6	11·84	0·84	0·66	4·73
7	13·71	0·83	0·69	6·56
8	15·71	0·82	0·72	8·51

TABLE 1

10. The measurements presented were made 1030 mm downstream of the perturbation generating the spot. The perturbation trajectories deduced from this figure suggest that the ensemble-averaged spot perturbs the laminar flow in a manner which would have been achieved by a large single vortex. The celerity of the interface was determined from figure 4, as discussed previously, and is given in table 1 for the elevations at which measurements are available.

The arrows shown in figure 11 (*a*) represent the velocity vectors relative to the leading interface. The slope of the velocity in this figure is stretched by the same ratio as the slope of the interface:

$$\frac{V}{U} = \frac{\Delta y}{\Delta x} = \frac{\Delta y}{U_{\mathrm{LE}}\,\Delta t}.$$

Each tick-mark on the abscissa represents either a timescale equivalent to 2 ms or a velocity scale of 2 m/s. Each tick-mark on the ordinate represents a vertical distance of 1 mm or a component of velocity

$$\Delta V = \frac{1}{U_{\mathrm{LE}}}\left(\Delta U \frac{\Delta y}{\Delta t}\right) \Big/ \text{tick-mark}.$$

The vertical velocity scale thus changes with U_{LE} in accordance with table 1. The scale is, however, stretched by a factor of approximately 9:1, while the actual distances are stretched by 18:1. The same procedure was used in figure 11 (*b*) relative to the trailing interface.

One may integrate (either graphically or numerically) the relative velocity component normal to the interface and obtain the average distribution of entrainment on the plane of symmetry (table 2): even a small angle between the ensemble-averaged velocity vector and the interface may represent a region in which the rate of entrainment is significant.

The first three rows in table 2 refer to results obtained by Zilberman (1981), the results of CCD are shown for comparison in the fourth row. The measured data indicates that the leading interface contributes approximately 40% to the total entrainment estimated in this way. The amount of fluid entrained under the 'overhang' (segment 1–2) is approximately equal to the amount of fluid entrained by segment 2–3. The ratio of entrainment between the leading and trailing interface corresponds approximately to the ratio of the lengths of these ensemble-averaged interfaces, suggesting perhaps that both are equally active in the entrainment process.

The ensemble-averaged perturbation velocity component normal to the surface can be calculated from the U-component by assuming that the average flow is two-dimensional (i.e. $(\partial W/\partial z)_{z=0} = 0$). The calculated perturbation vectors agree fairly well with the overall measured pattern (figure 10). Near the trailing interface, however, the calculated V was smaller than measured. The velocity vectors relative to the leading and trailing interface are shown in figure 12. The scale used in this figure is identical with the scale in figure 11, providing a direct comparison between the measured and calculated data. The relative entrainment by the trailing interface is much stronger if one considers the calculated V rather than the measured one. The calculated results are also tabulated in table 2. The calculated distribution of entrainment agrees fairly well with the calculated results of CCD. The apparent inactivity of the upper portion of the leading interface stems probably from the fact that the effects of the surrounding laminar boundary layer are neglected in the calculation.

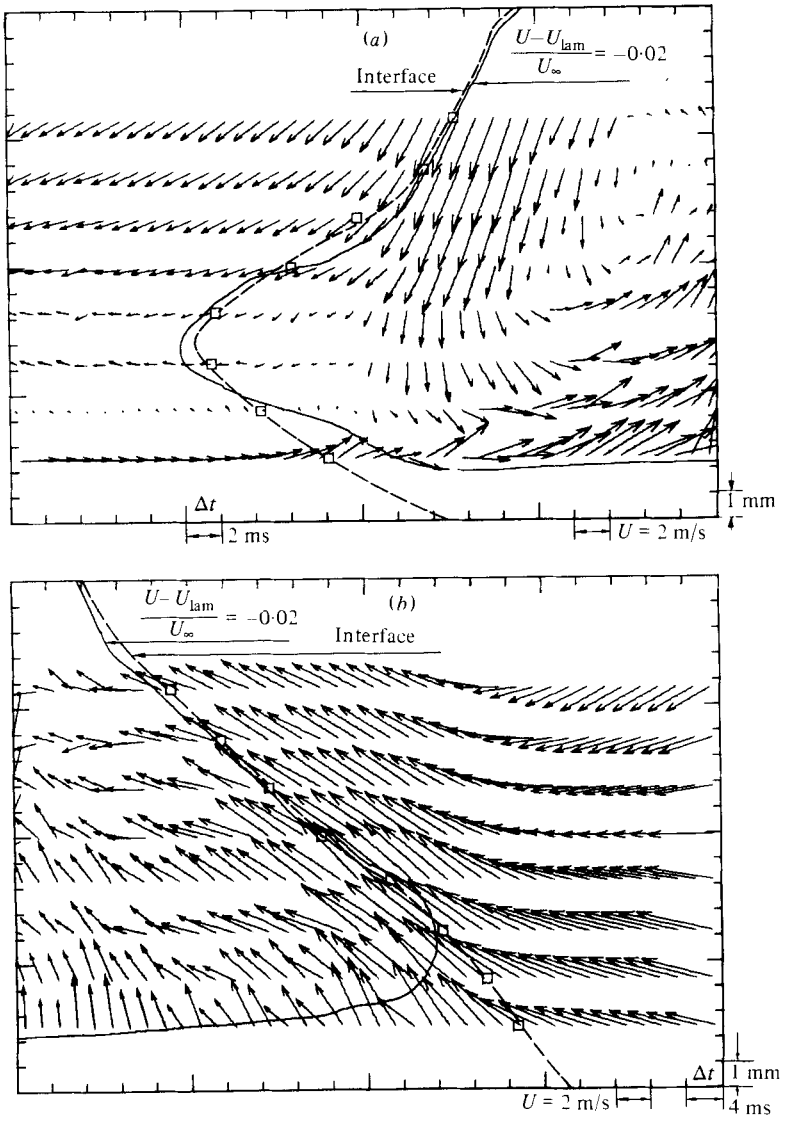

FIGURE 11. (*a*) Velocity vectors relative to the leading interface. (*b*) Velocity vectors relative to the trailing interface. See text for scales.

	Measured			Calculated		
Boundary definition	Segment 1–2	Segment 2–3	Segment 3–4	Segment 1–2	Segment 2–3	Segment 3–4
Interface	21 %	19 %	60 %	15 %	5 %	80 %
2 % (perturbation)	22 %	14 %	64 %	16 %	6 %	78 %
3 % (contours)	22 %	22 %	56 %	—	—	—
CCD	—	—	—	16 %	5 %	79 %

TABLE 2

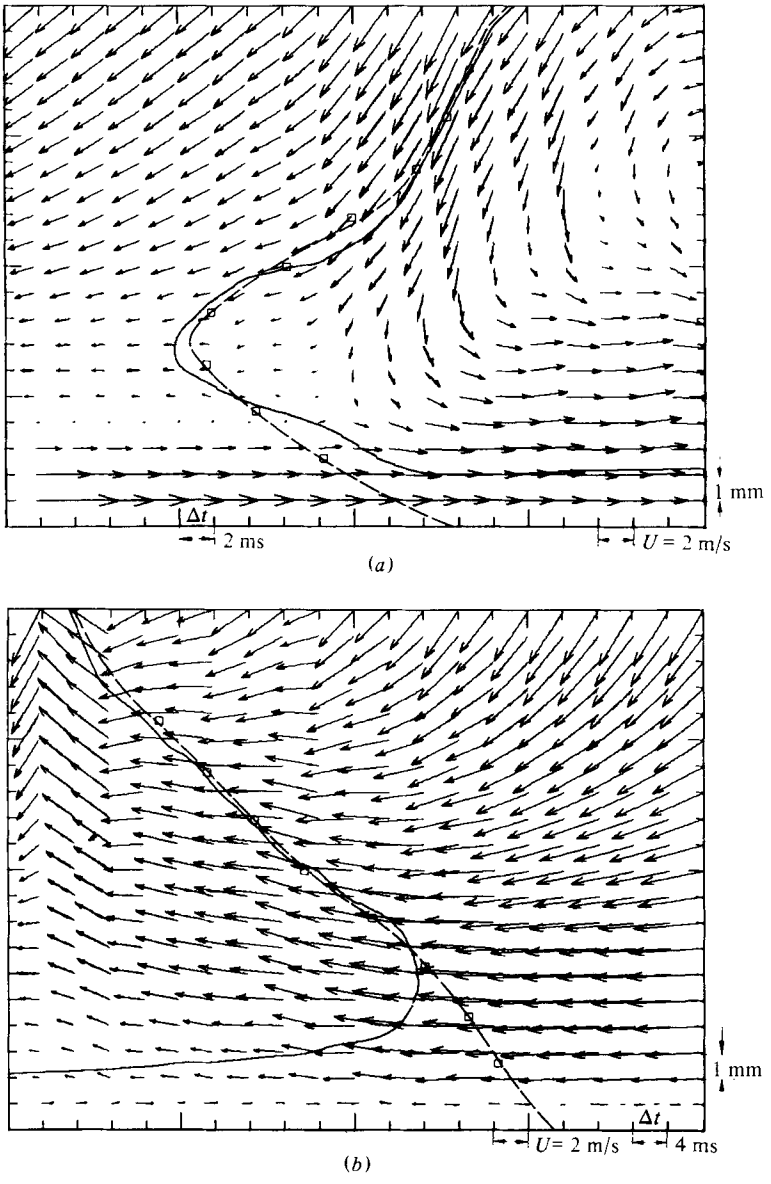

FIGURE 12. (*a*) Calculated vectors relative to the leading interface. (*b*) Calculated vectors relative to the trailing interface. See text for scales.

2.2. *The effect of Reynolds number*

The laminar boundary layer that provides the medium for the generation of the spot was not considered in the previous discussion. The thickness of this layer introduces another lengthscale, whose effect was never carefully investigated because most of the detailed experiments were carried out at one free-stream velocity and because the perturbation generating the spot was fixed in space.

When the experiments discussed in §2.1 were repeated at a free-stream velocity of 19 m/s, some differences were noticed. By plotting the same features as in figure 3, it appears that:

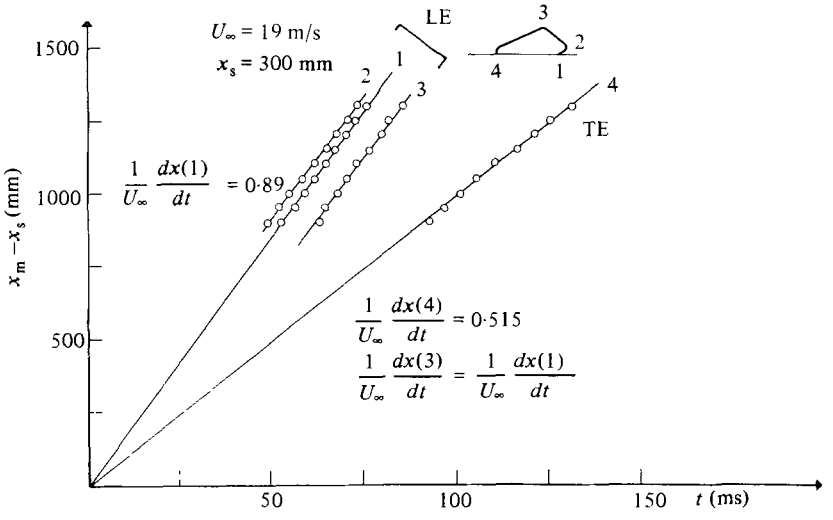

FIGURE 13. The celerity of some distinguished features of the spot.

(i) the streamwise component of celerity of the leading interface near the surface remained unchanged (i.e. $U_{LE} = 0{\cdot}89U_\infty$), but the streamwise component of locus 3 is also $0{\cdot}89U_\infty$;

(ii) the trailing interface slows down near the surface to $U_{TE} = 0{\cdot}515U_\infty$;

(iii) the various virtual origins of the flow move upstream (figure 13);

(iv) the dimensionless ratio between the length of the spot and its duration changed slightly, i.e.

$$\frac{l(x_m - x_0)}{U_\infty^2 \Delta t(t_m - t_0)} = 0{\cdot}43,$$

where x_0 and t_0 are at the intersection of loci 1 and 4.

The reduction in the celerity of the trailing interface near the surface was significant, and could not be attributed to experimental error. The same trend was observed in transitional pipe flow, where the velocity of the trailing edge of the slug decreased monotonically with increasing Re (Wygnanski & Champagne 1973). Since the difference in the celerity of the leading and trailing interfaces is associated with the rate of growth of the spot, the latter was investigated in detail near the surface of the plate. The actual length of the spot near the solid surface can be determined by two hot-wire probes separated by a distance corresponding to the spot length. Whenever the separation distance is correct, the trailing interface as detected by the first probe occurs simultaneously with the leading interface seen by the second probe. Because this determination is possible in a statistical sense only, one may determine the probe separation from ensemble-averaged data of a single wire and thus avoid undesirable effects of probe interference. Repeating the same measurement at numerous distances downstream of the spark, it appears that the spots grow linearly with x (x being the distance between the leading edges of the spots and their virtual origin on the surface) and their rate of growth dl/dx can be plotted for various Reynolds numbers based on the conditions at the spark (figure 14). Two spark positions were considered; one at $x_s = 300$ mm and the other at $x_s = 600$ mm from the leading edge, while the velocities ranged from 5 to 19 m/s. The streamwise rate

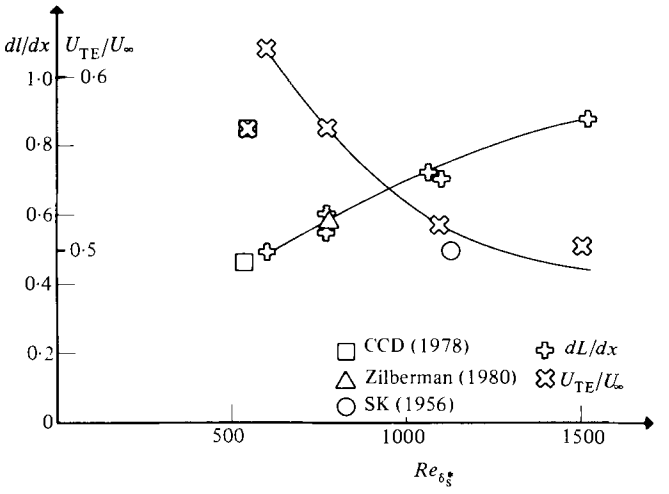

FIGURE 14. The longitudinal rate of growth of the spot and the dependence of U_{TE} on $Re_{\delta_s^*}$.

of growth of the spot strongly depends on Re, and doubles as $Re_{\delta_s^*}$ at the spark location is increased from 500 to 1500. The celerity of the trailing interface is also plotted in figure 14, indicating a continuous reduction of U_{TE} with increasing $Re_{\delta_s^*}$. In the range of $Re_{\delta_s^*}$ considered, the celerity of the trailing interface varies from $0{\cdot}62U_\infty$ to $0{\cdot}5U_\infty$. The celerity of the leading interface is independent of $Re_{\delta_s^*}$ at the spark. The ratio $l(x_m - x_0)/U_\infty^2 \Delta t(t_m - t_0)$ is also dependent on Re, and varies between 0·43 and 0·51 for the range of Re considered. Three data points taken from other experiments are shown in figure 14 for comparison. One was taken from CCD, who had a slight pressure gradient on their plate; the other was measured by Zilberman (1981) in the wind-tunnel facility at Tel-Aviv University, and the third point was measured by Schubauer & Klebanoff (1956).

The spanwise rate of growth of the spot is almost independent of $Re_{\delta_s^*}$ at the spark, as may be observed from the slope of the lines drawn in figure 15. The maximum spanwise rate of spread corresponds to an angle of 10°, while the minimum corresponds to 9·3°. The location of the hypothetical origin of the flow in the (x, z)-plane *depends on the free-stream velocity more than it does on the location of the spark*, and does not simply scale with $Re_{\delta_s^*}$. For all cases considered, $Re_{\delta_s^*} > 450$, which is regarded as the critical Reynolds number below which all small disturbances should decay. The initial lateral growth of the spot is slow at low values of $Re_{\delta_s^*}$, but the asymptotic state appears to be independent of Reynolds number.

In attempting to scale the spot geometry, one has to consider three apparent origins of the flow:

(i) relating time to streamwise distance;

(ii) relating the local boundary-layer thickness to the initial thickness at the spark;

(iii) relating the rate of growth in the spanwise direction to the velocity and Reynolds number of the flow.

The rate of growth of the spot in all three directions is also different.

(i) The length of the spot (in the x-direction) increases linearly with downstream distance and its rate of growth dl/dx increases almost *linearly with* $Re_{\delta_s^*}$.

(ii) The height of the spot (in the y-direction) increases with x at a rate similar to the growth of the turbulent-boundary-layer thickness. Assuming a power-law

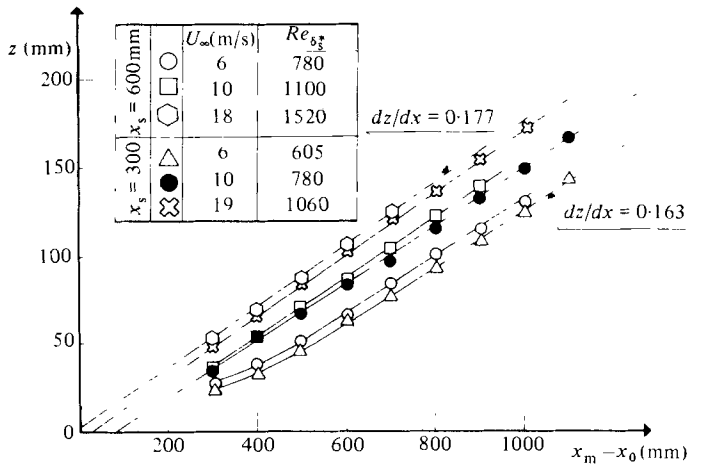

FIGURE 15. The spanwise growth of the spot for various $Re_{\delta_s^*}$.

relationship, it implies that, for a given free-stream velocity, the height of the spot increases proportionally to $x^{0.8}$. This rate of growth is *weakly dependent on Re*.

(iii) The spreading rate of the spot in the z-direction increases linearly with x, *irrespective of Re*, provided that the latter is large enough.

Thus the spot cannot be described as a universally self-similar structure growing conically from a single origin irrespective of $Re_{\delta_s^*}$.

The constancy of the relationship between temporal and spatial velocity records applies equally well to different Reynolds numbers as it did to the data shown in figure 6. The proportionality constant, however, depends on $Re_{\delta_s^*}$ because the streamwise rate of growth of the spot is dependent on $Re_{\delta_s^*}$ and the difference between the celerity of the leading and trailing interface also depends on Re.

The borders of ensemble-averaged spots, when plotted using the variables suggested previously for $U_\infty = 6$ m/s and 19 m/s, are fairly self-similar for each $Re_{\delta_s^*}$, justifying the choice of the scaling parameters.

There are, however, some obvious Reynolds-number effects. A comparison at a given distance from the spark reveals the following.

(i) The maximum height of the spot (point B) in figure 16 (a) is approximately $0{\cdot}75\delta_T$, while in figure 16 (b) it is $0{\cdot}9\delta_T$. For $Re_{\delta_s^*} = 1500$, the maximum height of the spot is $0{\cdot}95\delta_T$. The temporal (or spatial) position at which the spot attains its maximum height is given by $X \approx 1{\cdot}22$ for all Re considered.

(ii) The height of the 'overhang' (i.e. the most-forward location on the spot boundary, point A) does not depend on Re, buts its streamwise location depends weakly on Re and occurs at $X > 0{\cdot}94$ in the range of Re considered.

(iii) The location of the most-rearward $-2\,\%$ velocity perturbation contour (point C in figure 16) moves closer to the surface with increasing Re (from $Y = 0{\cdot}2$ in figure 16 (a) to $Y = 0{\cdot}15$ in figure 16 (b)), while at the same time occurring at larger values of X.

The effect of $Re_{\delta_s^*}$ on the flow field in the spot can be noticed whenever contours of velocity perturbation are plotted.

The region of strongest defect of velocity occurs in figure 16 (a) at an elevation corresponding to $\frac{1}{3}$ of the total height of the spot and $\frac{1}{2}$ of its length. The corresponding

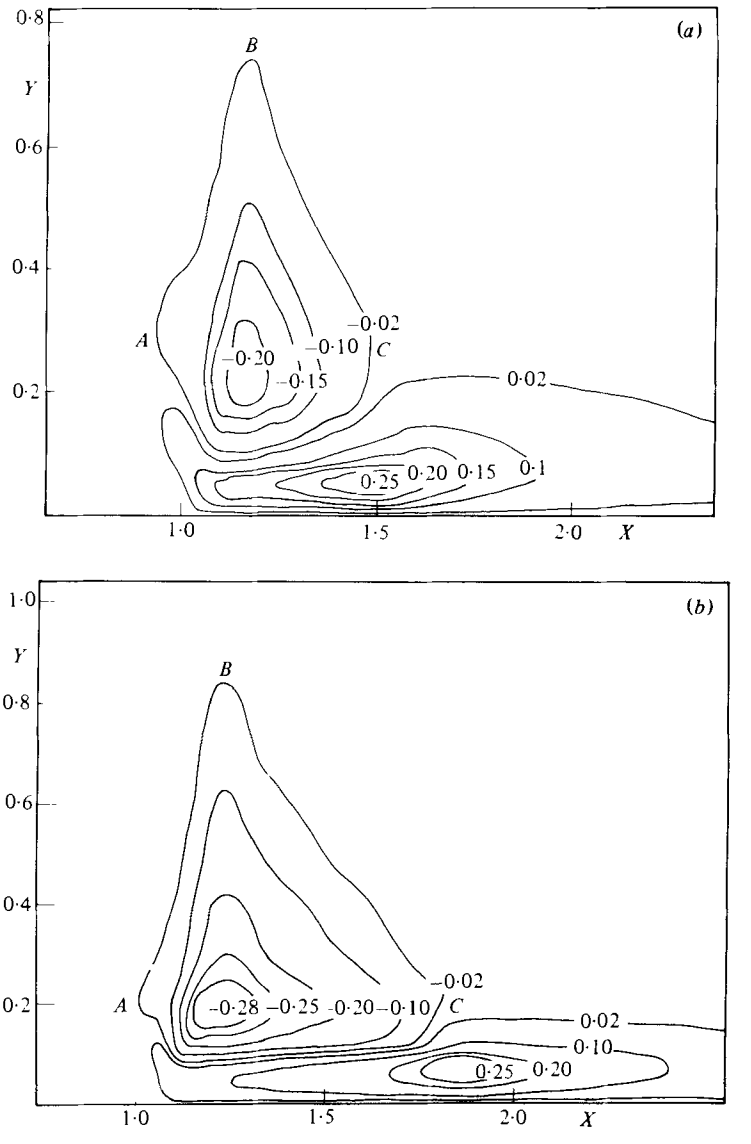

FIGURE 16. (*a*) Velocity perturbation at $U_\infty = 6$ m/s, $x_m - x_0 = 1000$ mm. (*b*) Velocity perturbation at $U_\infty = 19$ m/s, $x_m - x_0 = 1000$ mm.

location in figure 16(*b*) occurs at an elevation of 22 % of the height of the spot and 30 % of its length (i.e. closer to the leading interface of the spot). The relative height of the 'calmed' region behind the spot extends to 30 % of the spot height in figure 16(*a*) and only to 20 % of the height in figure 16(*b*). The streamwise distance between the highest velocity-defect region and maximum velocity-excess region is also increased with increasing $Re_{\delta_3^*}$.

Thus far, the entire discussion of the shape of the spot and the rate of its growth was based on ensemble-averaged data. The averaging process eliminates all fluctuations that occur randomly within the spot and gives the impression that its boundaries are smooth. The picture of a 'tagged' spot (insert in figure 18) indicates

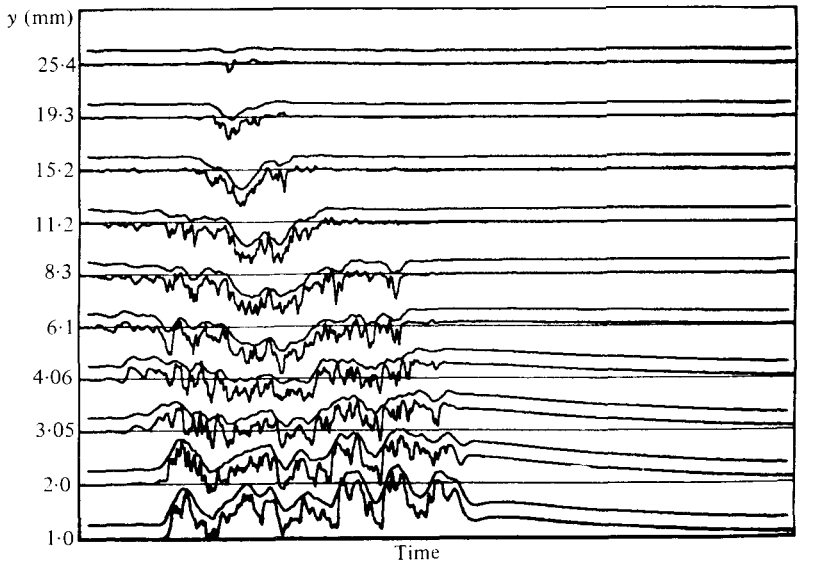

FIGURE 17. A single record of velocity perturbation measured at $U_\infty = 6$ m/s, $x_m - x_0 = 940$ mm.

clearly that the free interface between the turbulent and non-turbulent fluid is deeply corrugated, implying that the spot contains a finite number of large coherent structures. A record of the streamwise component of the velocity perturbation taken at $U_\infty = 6$ m/s and $x_m - x_0 = 940$ mm is shown in figure 17. Each velocity record was low-pass filtered digitally and replotted on the same figure for comparison, after being slightly displaced in the vertical direction. The filtering operation did not remove the low-frequency oscillations, which are coherent across the entire spot and can be followed from the solid surface to the outer interface. Contours of constant velocity perturbation were replotted from the records shown in figure 18 using the same techniques as for the ensemble-averaged data (figure 9). The velocity-perturbation contours indicate that the flow for the individual realization can still be described by a region of excess velocity near the surface and a region of velocity defect further away. The largest perturbation of velocity is $U - U_{\text{lam}}/U_\infty = +0{\cdot}4$, representing an increase of 30% over the ensemble-averaged data.

The boundaries of the spot resemble the photograph shown in the insert in figure 18. One may distinguish roughly five cellular eddy structures in the spot, which are coherent across its entire height. These eddies are separated by deep crevasses in which non-turbulent fluid is trapped.

CCD suggested that the spot entrains most of the non-turbulent fluid by a process they called 'nibbling', namely the propagation of a thin interface into the non-turbulent fluid by viscous diffusion of vorticity. The 'nibbling' process is dominant whenever the interface is fairly smooth, as it appears in the ensemble-averaged data. In the single realization the non-turbulent fluid may be engulfed between adjacent large-scale structures, allowing the relatively slow process of diffusion by smaller scales to act within the folds of the large eddies. The calculations of entrainment on the plane of symmetry cannot account for the rapid rate of growth of the spot, suggesting that there should be another mechanism involved. Measurements outside the plane of symmetry (Amini 1978; Perry, Lim & Teh 1981; Wygnanski 1981*a*, *b*) indicate that the spot contains a fairly orderly array of structures aligned in the

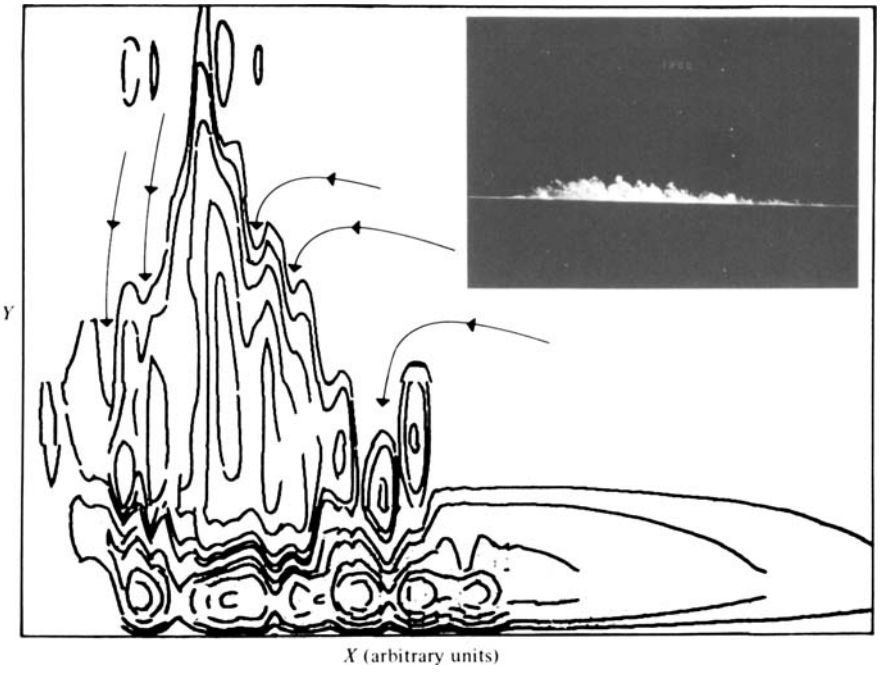

FIGURE 18. Velocity perturbation contours corresponding to the record shown in figure 17. The original of the photograph shown in the insert is from Gad-el-Hak *et al.* (1980) (see also Gad-el-Hak *et al.* 1981).

streamwise direction. Since these eddies are situated in preferred spatial locations within the spot (at least in the early stages of its development) they were even educed by a simple ensemble-averaging procedure. The mere existence of this substructure along the span of the spot suggests that the entrainment in the spanwise direction may be of major significance. More sophisticated analysis of the data (Wygnanski 1981*b*) revealed that the spot contains numerous 'hairpin' eddies arranged in an 'arrowhead' formation. The rapid rate of spread of the spot is attributed in part to the destabilization of the surrounding boundary layer and the continuous addition of hairpin eddies at the rear (upstream) edge of the spot. For this reason the celerity of the trailing interface is much lower than the celerity of the leading (downstream) interface.

'Hairpin' eddies generated near the wingtips of the spot are responsible for the spanwise spreading of the spot. Since these eddies most probably originate from the breakdown of Tollmien–Schlichting waves (Wygnanski *et al.* 1979), a threshold Reynolds number must be exceeded for the initial breakdown to occur. Beyond this Re, the rate at which the hairpin eddies are produced appears to be independent of Re. Thus the rate of spread of the spot in the spanwise direction is almost constant independent of $Re_{\delta_0^*}$ (figure 15).

Near the plane of symmetry of the spot the 'hairpin' eddies are crowded, thus the mere generation of these eddies cannot be solely responsible for the longitudinal growth of the spot. These large eddies may interact with one another and may get strained by the mean velocity field. Thus the elongation of the spot in the streamwise direction is not well understood; furthermore, the wave packet following the spot was not clearly identified in this region. However, if straining of the hairpin eddies

contributes to the elongation of the spot then the process should be dependent on *Re*.

The tip of the spot (i.e. its maximum elevation above the solid surface) is surrounded by turbulent eddies in the (x, z)-plane, and it protrudes into the potential fluid above the laminar boundary layer. It comes as no surprise that its rate of growth is equivalent to the rate at which a comparable boundary layer thickens.

3. Conclusions

It is established that the size of the transitional spot in a Blasius boundary layer depends either on its distance from the source or on the time elapsed from its initiation. The two variables, however, are related as long as the free-stream velocity and the location of the perturbing source are held constant. The rate of growth of the spot and the location of its apparent origin differ for each of the three principal directions. The dependence of the size and shape of the spot on the Reynolds number and on the thickness of the surrounding laminar boundary layer limits the usefulness of a single similarity transformation.

Finally, the physical process of entrainment cannot be satisfactorily explained from an ensemble-averaged picture of the spot, nor can it be explained on the basis of measurements made on the plane of symmetry alone.

This research was sponsored in part by the U.S. Air Force Office of Scientific Research under grants 76-3094, 77-3275. Experiments were carried out at the University of Southern California during the summer of 1979 and at Tel-Aviv University. Our deepest thanks go to Mrs Bette Lewis, who has typed this manuscript so many times.

REFERENCES

AMINI, J. 1978 Ph.D. thesis, Institut de Mécanique de Grenoble: to be published in *Phys. Fluids.*

CANTWELL, B., COLES, D. & DIMOTAKIS, P. 1978 *J. Fluid Mech.* **87**, 641.

COLES, D. & BARKER, S. J. 1975 In *Proc. Project SQUID Workshop on Turbulent Mixing in Non-Reactive and Reactive Flows* (ed. S. N. B. Murthy). Plenum.

GAD-EK-HAK, M., BLACKWELDER, R. F. & RILEY, J. J. 1980 In *Laminar–Turbulent Transition* (ed. R. Eppler & H. Fasel), p. 297. Springer.

GAD-EL-HAK, M., BLACKWELDER, R. F. & RILEY, J. J. 1981 *J. Fluid Mech.* **110**, 73.

KOVASZNAY, L. S. G., KOMODA, H. & VASUDEVA, B. R. 1962 In *Proc. Heat Transfer and Fluid Mechanics Institute.* Stanford University Press.

PERRY, A. E., LIM, T. T. & TEH, E. W. 1981 *J. Fluid Mech.* **104**, 387.

SAVAS, O. 1979 Ph.D. thesis, California Institute of Technology.

SCHUBAUER, G. B. & KLEBANOFF, P. S. 1956 *NACA Rep.* no. 1289.

WYGNANSKI, I. 1981*a* In *The Role of Coherent Structures in Modeling Turbulence and Mixing* (ed. J. Jimenez). Lecture Notes in Physics, vol. 136, p. 304. Springer.

WYGNANSKI, I. 1981*b* In *Proc. 7th Biennial Symp. on Turbulence – Rolla, Missouri.*

WYGNANSKI, I. & CHAMPAGNE, F. H. 1973 *J. Fluid Mech.* **59**, 281.

WYGNANSKI, I., HARITONIDIS, J. & KAPLAN, R. E. 1979 *J. Fluid Mech.* **92**, 505.

WYGNANSKI, I., SOKOLOV, M. & FRIEDMAN, D. 1976 *J. Fluid Mech.* **84**, 785.

ZILBERMAN, M., WYGNANSKI, I. & KAPLAN, R. E. 1979 *Phys. Fluids Suppl.* **20**, S258.

ZILBERMAN, M. 1981 Ph.D. thesis, School of Engineering, Tel-Aviv University.